FORUM GEOGRAFI
ISSN: 0852-0682 | E-ISSN: 2460-3945
HTTPS://JOURNALS.UMS.AC.ID/INDEX.PHP/FG/

Research article

Modelling of Soil Erosion Susceptibility Using the Multi-Influencing Factor Method in the Amizmiz Basin, Morocco

Saloua Agli [1*], Algouti Ahmed[1], Algouti Abdellah[1], Farah Abdelouahed[1,2], Moujane Said[1], Aboulfaraj Abdelfattah[1], El ghouat Akram[1,3]

[1] Department of Geology, Geosciences Geotourism Natural Hazards, and Remote Sensing Laboratory Faculty of Sciences Semlalia, Cadi Ayyad University, Marrakech, Morocco
[2] GEOANLYSIS, engineering consulting office of Geological, geophysical, and environmental services, Marrakech, Morocco
[3] Interuniversity Institute for Earth System Research (IISTA), University of Granada, Granada 18006, Spain

[*)] Correspondence: saloua.agli@gmail.com

Citation:
Saloua, A., Ahmed, A., Abdellah, A., Abdelouahed, F., Said, M., Abdelfattah, A., Akram, E. G. (2024). Modelling of Soil Erosion Susceptibility Using the Multi-Influencing Factor Method in the Amizmiz Basin, Morocco. Forum Geografi. 38(3), 343-357.

Article history:
Received: 7 Agust 2024
Revised: 14 October 2024
Accepted: 16 October 2024
Published: 11 December 2024

Abstract

In the Western High Atlas of Morocco, soil loss caused by hydraulic erosion is a serious environmental issue that has led to the destruction of arable land and the feeding of surface water with large solid loads, resulting in major flood damage and the silting of dams. This study aims to identify areas vulnerable to hydraulic erosion in the Amizmiz watershed in the Western High Atlas to facilitate effective management of natural resources. The methodology adopted in this study is based on the multi-influencing factor (MIF) method coupled with remote sensing and geographic information system (GIS) data. The resulting erodibility map shows that areas with low to very low erosion potential represent 13% and 6% of the watershed, respectively, occupying the downstream and eastern parts of the basin, whereas 62% of the basin is classified as medium-risk. The remaining 19% of the watershed comprises high-risk areas, which are generally located in the axial and western zones. The validation value (AUC) obtained from the ROC curve is 0.78, confirming the sufficient predictive capacity of the MIF model for identifying areas vulnerable to hydraulic erosion in the Amimiz watershed.

Keywords: Amizmiz watershed; hydraulic erosion; remote sensing; GIS; Multi-influencing factor.

1. Introduction

Soil loss is a serious environmental problem worldwide (Le Bissonnais *et al.,* 2002), hindering the progress of sustainable development (Liu *et al.,* 2018). Soil loss leads to reduced soil productivity, and consequently, decreased crop yields, particularly in developing countries. Several interdependent processes contribute to this phenomenon, including topography, soil behaviour and texture, rainfall erosivity, runoff, vegetation cover, and cultural and anthropogenic activities (Kirkby *et al.,* 2003). Soil erosion occurs when rainwater can no longer infiltrate the soil. In other words, when the precipitation intensity exceeds the infiltration capacity of the soil (Le Bissonnais *et al.,* 2002), runoff is triggered, resulting in several forms of erosion: linear erosion in talweg areas, parallel erosion, and gully erosion.

Moreover, soil loss poses threats to food security, water reservoirs, and agriculture in Morocco. This phenomenon also reduces the capacity of dams to store water. The Food and Agriculture Organization (FAO) and the World Resources Institute (WRI) have ranked Morocco among the 19 countries expected to be most threatened by water stress by 2040 (Haitami *et al.,* 2017). According to studies conducted by Morocco's Forestry Department (HCEFLCD) in collaboration with the FAO, hydraulic erosion reduces the capacity of dams to 75 million m^3/y (Innan *et al.,* 2012) due to silting problems (Nouaim *et al.,* 2023). This is mainly a result of the intense degradation of Moroccan soils caused by overgrazing and deforestation, compounded by the impact of droughts, which have increased over the years owing to climate change, making these lands more vulnerable to erosion. Therefore, it is imperative that Morocco take all necessary measures to mitigate the negative effects of hydraulic erosion. Water resources and soil fertility must be preserved.

In the Amizmiz Basin, which is located in the western High Atlas of Morocco, soil erosion is a serious problem owing to the topographical and lithological characteristics of the area coupled with intense short-duration rainfall and long periods of drought. The Lalla Takerkoust Dam, located at the outlet of the Amizmiz Basin, has experienced a 20% decrease in storage capacity over the last 20 years due to silting. Therefore, to manage water resources in the Amizmiz Basin, it is important to model hydraulic erosion, which requires describing the complex interaction of several factors affecting the hydraulic erosion process. To achieve this objective, high-performance tools must be used to estimate the areas vulnerable to erosion. These tools are based on remote sensing and geographic information systems (GIS) and are coupled with empirical and statistical

methods (Ourhzif *et al.,* 2020; Kirkby *et al.,* 2004), which use models adapted to the local conditions of the study area considering the available data and their feasibility for the model used.

Recent studies have increased the applications of GIS coupled with models for qualitative and quantitative estimations of soil erosion. For example, Oudchaira *et al.* (2024), Nouaim *et al.* (2023), Fartas *et al*. (2022), Saoud *et al*. (2022), Kabili *et al.* (2022), and Khemiri *et al.* (2021) applied the GIS-integrated RUSLE model to estimate the soil loss in mountainous areas of Morocco, Algeria, and Tunisia, highlighting the efficiency of satellite and geospatial data in mapping erosion risks. Elbadaoui *et al.* (2023) applied the erosion potential model (EPM) to quantify soil loss in the Toudgha River watershed in the central High Atlas of Morocco by combining remote sensing data with field data related to soil erodibility. Soil erodibility mapping studies have also been conducted based on the permanent availability of pastureland/carrying capacity of agro-rangeland (PAP/CAR) model (Ziadi *et al.,* 2023; Elbadaoui *et al.,* 2023; Tahouri *et al.,* 2022; Fartas *et al.,* 2021). This model is designed to identify areas susceptible to soil erosion, particularly in regions where human activities such as urbanisation, deforestation, and agriculture exacerbate the erosion risk. Some studies have demonstrated the importance of using the multi-criteria decision method developed by Saaty in 1980 to model erosion-sensitive areas based on the contributions of GIS and remote sensing. Among these models is the analytical hierarchy process (AHP) model (Ebhuoma *et al.,* 2022; Khairuddin *et al.,* 2022; Farah *et al.,* 2022; Sutradhar *et al.,* 2021; Igwe *et al.,* 2020; Rajasekhar *et al.,* 2019; Lin *et al.,* 2017). The AHP model provides high flexibility by integrating geological, topographic, and climatic data into a clearly defined hierarchy to enhance the relevance of the results. Similarly, the multi-influencing factor (MIF) model is an analytical weighting method that can be used to assess and model the impacts of various environmental factors on natural phenomena. The MIF model is a very specific model known for its simplicity, as it assigns scores to the various factors involved in the erodibility process and does not require a complex hierarchical structure. The MIF model adapts effectively to regional specificities and the complex integration of factors (Forootan *et al.,* 2022).

In this study, the MIF technique was used to identify areas vulnerable to erosion by evaluating the combined effects of topographic, geological, structural, and anthropogenic factors. Scores were assigned to each factor based on their relative importance and correlations. These interactions define the degree of erodibility and help identify vulnerable zones. The MIF model plays a key role in informing decisions related to natural resource management as well as environmental protection and conservation efforts. The technique used to validate the accuracy of the MIF method has generally been based on field visits and comparisons between erodibility classes obtained by modelling hydraulic erosion and those obtained in the field. Validation data were processed using statistical software such as SPSS to obtain receiver operating characteristic (ROC) curves. Several studies have used ROC curves to validate the geospatial approach coupled with the AHP technique to achieve a good level of accuracy and applicability. On the other hand, other methods exist for validating this type of modelling, such as positive and negative predictive values, kappa, and the square root of means, (Yariyan *et al.,* 2020; Chen *et al.,* 2018).

2. Research Methods

2.1. Study area

The Amizmiz Basin is located on the northern flank of the ancient massif of the Central Western High Atlas in Morocco. It lies within the Marrakesh-Safi region, specifically in the province of Al Haouz, approximately 55 km southwest of Marrakesh city (Figure 1). The basin is oriented SW-NE between latitude 31°7'36.852 N and longitude 8°16'8.649 W with an area of approximately 173.5 km² and a perimeter of 86.525 km. It is traversed by the Amizmiz River, and its elevation ranges from 669 m to 3280 m upstream. The Amizmiz Basin is characterised by a semi-arid climate, with average annual precipitation of approximately 417 mm. Geomorphologically, the basin is characterised by rugged terrain, with deep gorges carved by rivers and steep hills featuring cliffs and escarpments.

The Amizmiz area exhibits a lithostratigraphic sequence ranging from the Palaeozoic to Meso-Cenozoic (Figure 2). The Palaeozoic (Figure 2 D, E) strata are composed of metamorphosed and deformed sedimentary terrains of Cambrian and Carboniferous ages. The Mesozoic is represented by sedimentary terrains ranging in age from the Lower Cretaceous to the Upper Cretaceous (Figure 2 C, B). The Tertiary period is represented by sedimentary terrains from the Eocene and Mio-Pliocene, characterised by abundant detrital formations that rest unconformably on the Upper Cretaceous terrains (Figure 3). The Quaternary is essentially represented by loose detrital formations of stony terraces with conglomeratic deposits (Figure 2 A) (Agli *et al.,* 2023; Ellero *et al.,* 2012; Ayad *et al.,* 1998; Vanguestaine *et al.,* 1983).

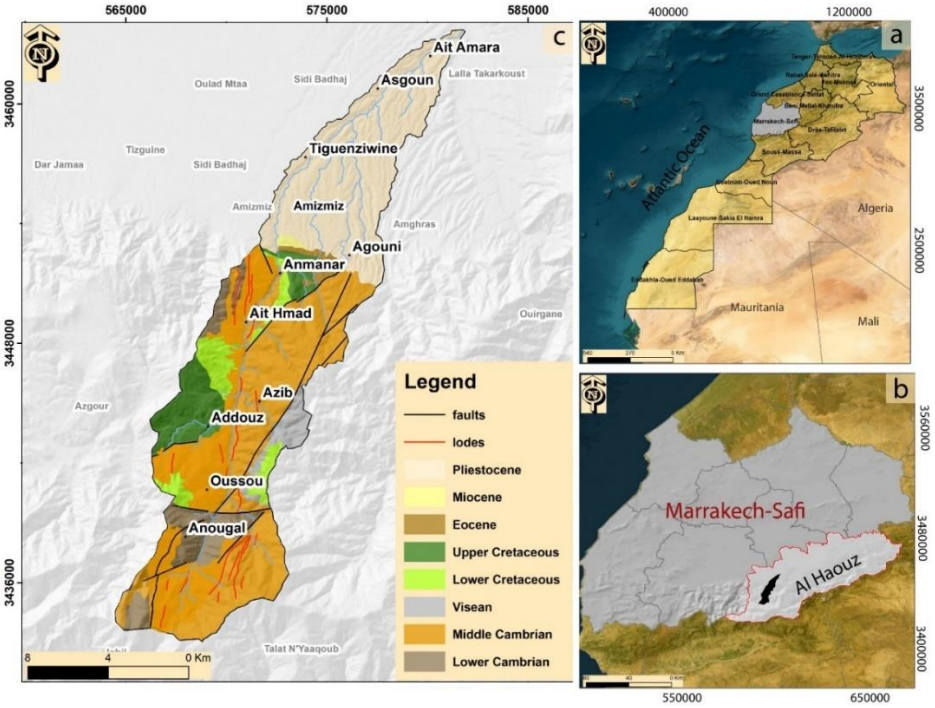

Figure 1. (a) Location of the study area in Morocco; (b) Location of the study area in the Marrakech-Safi region; (c) Simplified geological map of the study area.

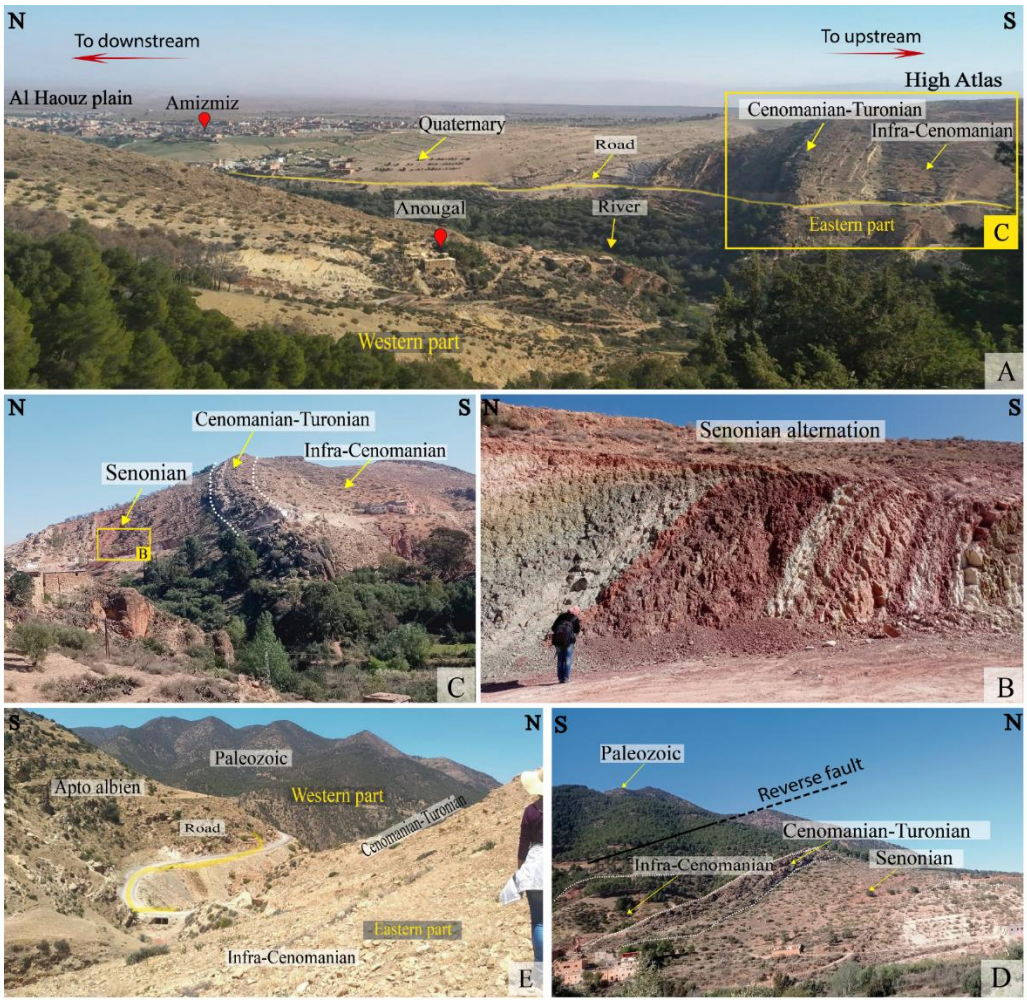

Figure 2. (A) Panoramic view of the geological formations in the study area; (B) Alternating Senonian formations; (C) Limestone massif bar of Cenomano-Turonian and Infra-Cenomanian age; (D) Limit between the Paleozoic and Meso-Cenozoic cover, with the reverse Amizmiz fault; (E) Limit between the Apto Albien and Infra-Cenomanian age.

2.2. Generation of thematic maps

The first step in this methodology involved describing the control factors (Table 1), while the second step focused on classifying and acquiring all of these factors, followed by assigning weights and integrating them into a GIS platform. Mapping the thematic layers of the factors required processing various remote sensing data and digital images (Figure 3). The lithology of the study area was mapped by digitising a geological map of Amizmiz at a scale of 1:100,000. A slope map was derived from the digital elevation model (DEM) with a resolution of 30 m. The land use map was generated from a Landsat 8 OLI image (LC08_L2SP_201038_20240309_20240309_02_T1) dated 9 March 2024, with a resolution of 30 m. Supervised classification was performed using the maximum likelihood algorithm. A rainfall map was generated by interpolating rainfall data from the study area over the past ten years.

The methodology adopted for mapping the vegetation density distribution was primarily based on the normalised difference vegetation index (NDVI), which is obtained from a combination of original radiometric data, specifically the near-infrared (NIR) and red (R) bands (Ke *et al.,* 2015). This index can be calculated using Equation 1:

$$NDVI = \frac{NIR-R}{NIR+R}. \quad (1)$$

To obtain the lineament map of the Amizmiz Basin, we treated the noisy appearance of the Landsat 8 OLI image by reducing the shimmer size using the "Lee" filter in the ENVI program. The next step was to identify existing discontinuities in the area by applying directional filters following principal component analysis (PCA). In this study, 0°, 45°, and 90° directional filters were applied to facilitate manual extraction of various structural lineaments. Manual extraction was performed through digitisation of the lineaments obtained after filtering (Moujane *et al.,* 2024; Farah *et al.,* 2022; 2021).

Table 1. Description of erodibility control factors.

Thematic layers	Materials Used	Justification of Indicators	Source
Geology	Geological map at a scale of 1/100,000	Lithological characteristics provide important information on the degree of soil erodibility. They include the compactness and degree of weathering of the rock, the presence of diaclase, joints, and faults.	(Ziadi, *et al.,* 2023; Elbadaoui *et al.,* 2023; Forootan *et al.,* 2022).
Lineament	Landsat 8OLI	Lineament density identifies highly fractured zones that represent areas most vulnerable to erosion. The presence of faults and fractures facilitates the degradation of the rocks, which becomes less stable. In addition, the infiltration of rainwater through these fractures and fissures also favours the chemical alteration of carbonate rocks.	
Slope	SRTM DEM (with 30 m resolution)	The length, shape, and especially slope inclination significantly influence the hydraulic erosion process. These parameters facilitate the creation of gullies and depressions on the soil surface. The erosion potential decreases on concave slopes compared with convex slopes where soil losses are much higher.	
NDVI	Landsat 8OLI	The vegetation cover plays a primordial role in the protection of soils against hydraulic erosion; a high density of vegetation cover favours the permeability of the soil and slows surface runoff, thus reducing soil erosion.	
Land use	Landsat 8OLI	Land use provides information about the landscape units of the study area, through which the protection and degradation levels of the soil can be determined. This reflects the role of anthropogenic factors in the vegetation cover, which plays a very important role in protecting the soil against hydraulic erosion.	
Precipitation	Data	In temperate zones, the combined action of precipitation and runoff has proven to be an effective means of mobilising fine particles from the soil surface. Therefore, the intensity of rainfall has an important role in the generation of risks and forms of erosion. Erosion depends on the rate of runoff and thus on the detachment and transport capacity of the runoff.	

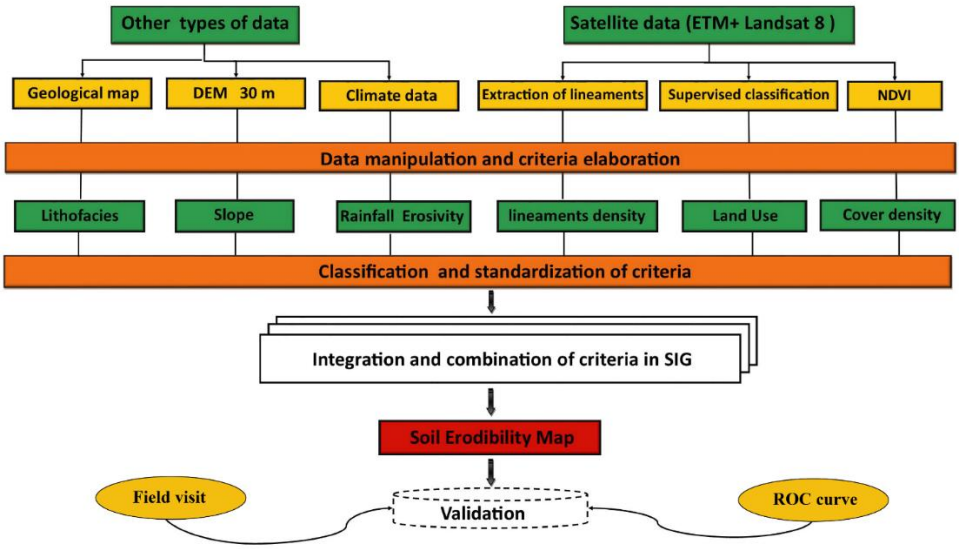

Figure 3. Organisational methodology adopted in the study area.

2.3. Multi-influencing factor (MIF) technique for analysis of priorities

The MIF technique adopted in this study is based on the complex interactions between criteria, and scores are assigned to different influencing factors. The MIF method was successfully applied in Iran by Forootan *et al.* (2022) in combination with fuzzy logic to evaluate the susceptibility to hydraulic erosion. In this approach, weights are assigned to each factor according to their importance, influence on soil erodibility, and resistance capacity of the different units. The interrelationship between the factors influencing soil erodibility is illustrated in the interaction schema (Figure 4), where two types of effects are identified based on the degree of influence each factor exerts on another (Mandal *et al.,* 2021; Sutradhar *et al.,* 2021), i.e. major effects and minor effects. Each major variable receives a score of 1 wt and each minor variable receives a score of 0.5 wt (Table 2).

Major effects are attributed to a factor when its influence on soil erosion is strong and direct. For example, lithology has three major effects (1+1+1) on lineaments, precipitation erosivity, and vegetation cover. Indeed, the nature of the lithology controls the degree of fracturing and the level of erosion caused by precipitation. Additionally, soil characteristics directly influence vegetation cover. Minor effects are attributed to a factor when its influence is relatively negligible but still present. For example, the same lithological factor has two minor effects on slope and land use. On gentle slopes, erosion remains low despite the high lithological sensitivity. Lithology can also sometimes inhibit anthropogenic protection. These interactions between lithology and other factors highlight their importance in determining erosion susceptibility. Other parameters are correlated in the same manner. Next, the weight of each influencing factor is calculated using Equation 2.

$$S = \frac{A + B}{\sum[A + B]} \times 100 \quad (2)$$

Subsequently, the weights of the individual factors are divided by the number of subclasses and distributed among the subclasses (Agli *et al.,* 2024; Mandal *et al.,* 2021; Sutradhar *et al.,* 2021). Because the highest-scoring influential subclass (Si1) is assigned the same weight as the parameter of concern (Pi), Equation 3 is defined.

$$Si1 = Pi \quad (3)$$

Then, the value of the weight of the factor (Pi) is divided by the total number of subclasses (nT), and the obtained value (Ai) is subtracted from the highest influential subclass (Si1). The resulting value is then attributed to the next-highest influencing subclass (Si2), yielding Equation 4.

$$S_{i2} = S_{i1} - \left[\frac{Pi}{nT}\right] \; when \; Ai = \frac{Pi}{nT} \quad (4)$$

Similarly, Si3 is calculated by subtracting Ai from Si2. This weight assignment procedure is repeated for the remaining subclasses (Tables 3, 4, and 5). For example, for the lithology factor, the conglomerate subclass is more vulnerable to erosion; therefore, it receives an initial weight of Si1 = 25 according to Equation 2. Subsequent subclasses receive progressively lower weights based

on their vulnerability to erosion. For instance, the subclass of pebbly and silty terraces and conglomerates receives a weight of Si2 = 23 by applying Equation 4. This process is repeated for each subclass, ranging from the most vulnerable to the least vulnerable, until reaching the most resistant formations, such as limestone, which does not promote erosion and therefore receives the lowest score (Si13 = 1).

Table 2. Major and minor effects of influencing factors and proposed relative rates and scores.

Influencing factor	Major effect [A]	Minor effect [B]	Relative rate [A+B]	Score of influencing factors
Lithology	1+1+1	0,5+0,5	4	25
Lineament (km/km²)	1+1	0,5+0,5	3	19
Land use	1	0,5	1,5	9
Slope (degree)	1	0,5+0,5	2	12
Rainfall erosivity	1+1+1	0,5	3,5	22
Cover density	1	0,5+0,5	2	12
Total	-	-	∑16	∑100

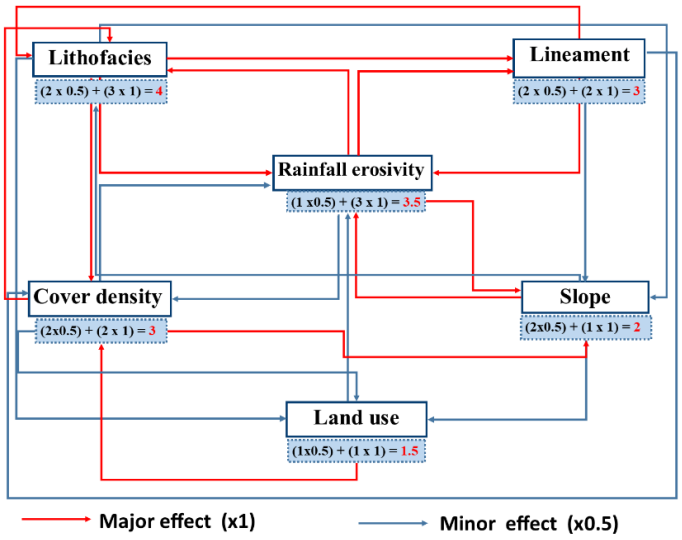

Figure 4. Schema of the interactions between factors influencing hydraulic erosion.

2.4. GIS processing

GIS software was used to create the final hydraulic erosion map by integrating six thematic maps using Equation 5.

$$SE = GLW.GLS + LMW.LMS + LUW.LUS + SW.SS + REW.RES + LCW.LCS, \quad (5)$$

where SE represents the soil erodibility; GLw represents the weight of geology, and GLS represents the score of the theme; LMw represents the weight of lineament, and LMS represents the score of the theme; LUw represents the weight of land use, and LUS represents the score of the theme; Sw represents the weight of the slope, and SS represents the score of the theme; REw represents the weight of rainfall erosivity, and RES represents the score of the theme; LCw represents the weight of land cover, and LCS represents the score of the theme.

3. Results and Discussion

3.1. Factors influencing soil erodibility

3.1.1. Lithology

In this study, the classification of the geological units was based on the relative degree of cohesion and resistance to erosion. The lithological map of the Amizmiz Basin allowed us to distinguish 14 principal geological units, which were classified according to the degree of erodibility of the materials into the four categories in Table 3: resistant, moderately resistant, vulnerable, and very vulnerable. The resistant lithological units are represented in the map (Figure 5a) by compact formations (volcanic rocks), comprising 6% of the basin area; 24% of the consolidated formations (marne, sandstone limestone, sandy marl, shell limestone, marly limestone, shale, etc.) are moderately resistant. Almost all of the basin is marked by unconsolidated to loose formations that are

located downstream of the study area; these formations are moderately vulnerable to vulnerable, comprising a percentage of 70%.

3.1.2. Lineaments

The density of fractures is expressed as the total cumulative length or number of fractures per unit. This density indicates the degree of fracturing of the rocks. The lineament density map of the Amizmiz Basin (Figure 5b) is classified into five units based on the intensity of fracturing and the degree of erosivity. From the lineament density map of the study area, we distinguish five classes (Table 3). Highly fractured areas are located in the upstream and central parts of the basin.

Table 3. Ranks and weights of the lithology and lineament density.

Factors	Parameters	Description	Theme weight	Score
Lithology	Pebbles, conglomerates	Very vulnerable	25	25
	Pebbly, silty terraces, conglomerates			23
	Argillites and siltites			21
	Schistose unit			19
	Grey schist			17
	Sandstone, marl, clay, gypsum	Vulnerable		15
	Clays, sandstones, conglomerates	Mildly resistant		13
	Greywackes shale, volcanic tuff			11
	Shell limestone, marly limestone			9
	Sandstone limestone, sandy marl			7
	Shales, orthoquartzites, mudstones with tuff			5
	Limestone, marl, clay, and sandstone			3
	Limestone bar	Resistant		1
Lineaments density	[0 - 1,32]	Very resistant	19	3
	[1,32 - 2,55]	Resistant		7
	[2,55- 3,74]	Mildly resistant		11
	[3,74 - 5,27]	Vulnerable		15
	[5,27 - 8,67]	Very vulnerable		19

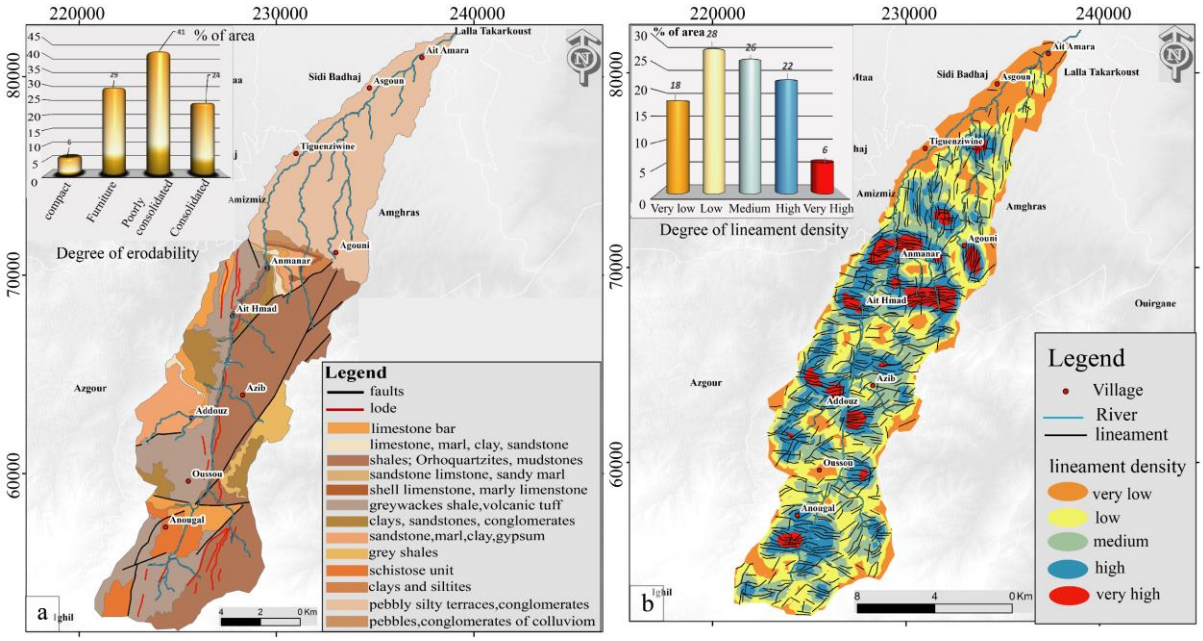

Figure 5. (a) Lithological map of the Amizmiz watershed and area percent corresponding to different degrees of erodibility of the material; (b) lineament density map and area percent corresponding to different degrees of lineament density.

3.1.3. Slope

Based on the slope map (Figure 6a), the slopes of the Amizmiz watershed are assigned to five classes (Table 4) according to the degree of inclination and length of the slope, which can influence the degree of soil erodibility. The low and very-low slopes are located in the downstream part of the basin and are estimated to comprise 47% of the watershed area. The highest slopes are located in the upstream part of the basin and comprise of 29% of the area. The centre is marked by slopes of medium degree, covering 24% of the basin area.

3.1.4. Cover density

The application of the NDVI allows us to map the density of the vegetation cover in the study area (Figure 6b); we distinguish five classes according to the degree and intensity of vegetation (Table 4). The obtained NDVI map shows that the vegetation cover is concentrated in the centre of the watershed around the river, where the density is maximal, whereas it is generally high to moderate in the eastern and western parts of the Amizmiz watershed.

Table 4. Ranks and weights of the slope and cover density.

Factors	Parameters	Description	Theme weight	Score
	[0 - 8,31]	Very resistant		0
Slope	[8,31 - 16,2]	Resistant		3
(Degree)	[16,02- 23,73]	Mildly resistant		6
	[23,73 - 31,65]	Vulnerable		9
	[31,65 - 51,73]	Very vulnerable	12	12
	[-0,05 - 0,04]	Non-protective	12	12
Cover density	[0,04 - 0,09]	Mildly protective		9
(NDVI)	[0,09 - 0,14]	Mildly protective		6
	[0,14 - 0,22]	Protective		3
	[0,22 - 0,43]	Highly protective		0

3.1.5. Rainfall erosivity

The rainfall map indicates the aggressiveness of rainfall in the study area. The rainfall intensity increases from downstream to upstream in the watershed (Figure 6c). By interpolating over 50 years of rainfall data, we observe that the rainfall varies from 320 to 480 mm, with the highest values recorded in the axial zone in the southern and western parts of the basin. Based on the degree of erosivity of precipitation in the Amizimz watershed, we distinguish five classes, as described in Table 5.

3.1.6. Land use

Table 5. Ranks and weights of land use and rainfall erosivity.

Factors	Parameters	Description	Theme weight	Score
	Water	Non-protective	9	9
	Dense forests	Highly protective		0
Land use	Planted drops	Mildly protective		7
	Urban areas	Non-protective		5
	Bare soils	Non-protective		7
	Open forests and agricultural areas	Protecteurs		3
	[10,32 - 80,12]	Very low		2
Rainfall erosivity	[80,12 - 170,4]	Low		7
	[170,4- 280,04]	Medium		12
	[280,04 - 400,89]	High		17
	[400,89 - 650,6]	Very high	22	22

The land use types in the Amizmiz watershed were classified using a supervised classification based on the maximum likelihood algorithm (Figure 6d). These classes were defined according to their distinct spectral signatures extracted from different bands of the Landsat 8 OLI sensor.

They were selected based on prior knowledge of the terrain and a high-resolution satellite image and then grouped into six categories (water, dense forests, open forests, crops, bare soil, and urban areas) based on their level of protection (Table 5). Dense forests are primarily located in the central part of the catchment, whereas open forests and cultivated areas are distributed over almost the entire surface area of the watershed. Urban areas, represented by buildings, are moderately prevalent in the sector. The amount of bare ground that is devoid of vegetation is also limited in the study area. The mapping also includes areas occupied by water, such as rivers and tributaries.

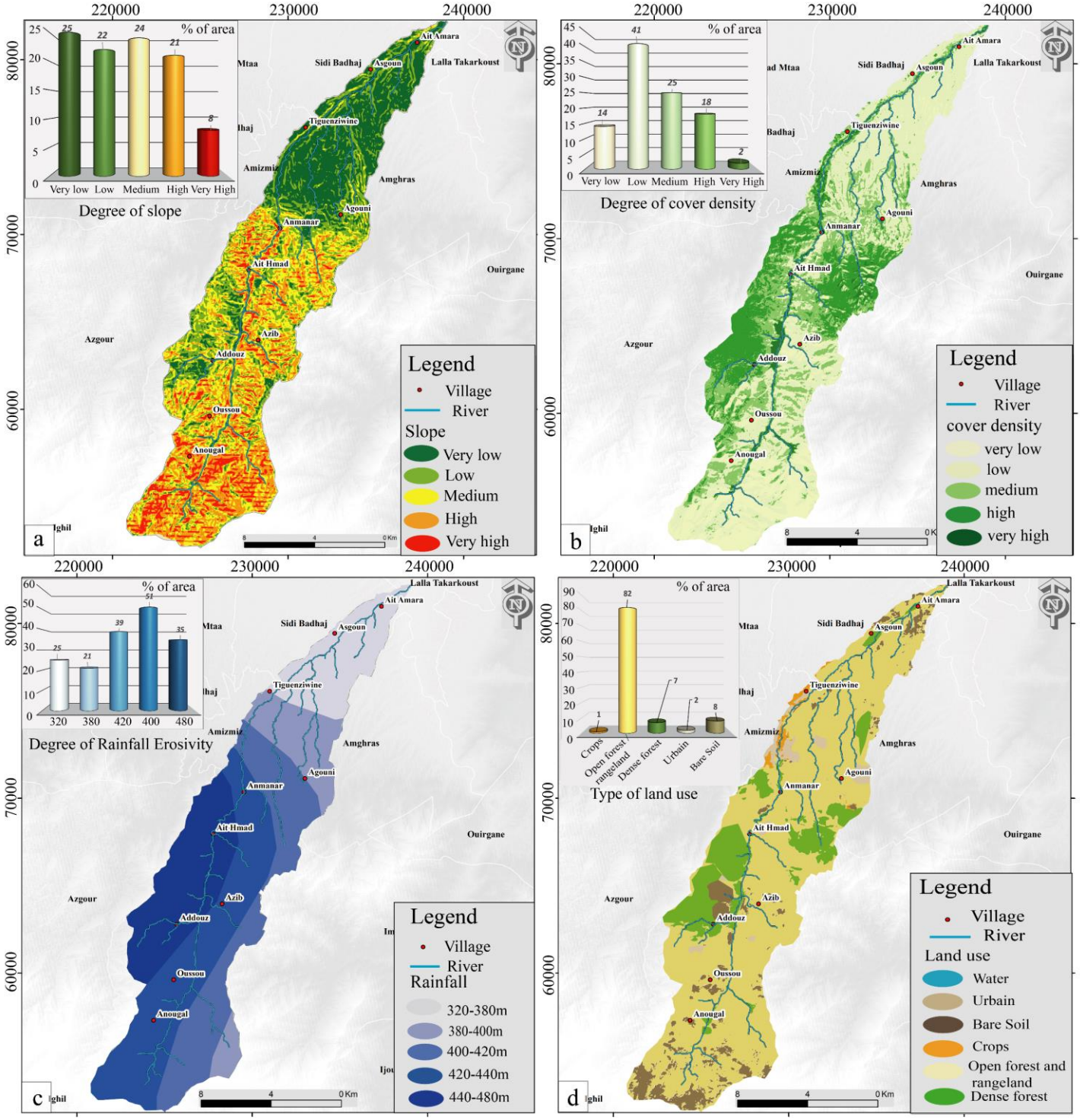

Figure 6. (a) Map of slopes and the slope degree as a percentage of the surface area; (b) NDVI map and area percent of different degrees of vegetation cover; (c) precipitation map and area percent of different degrees of rainfall erosivity; (d) land use map and area percent of different land use types.

3.2. Mapping of areas vulnerable to erosion

The soil erodibility map of the Amizmiz watershed (Figure 7A) created using the MIF method coupled with remote sensing and GIS indicates an unequal spatial distribution of vulnerability to

hydraulic erosion. Areas with high erodibility account for 19% of the study area. These areas are generally concentrated in the western part of the Amizmiz catchment area, from the axial zone to the centre. Most of these areas are characterised by a high erosivity of precipitation with highly fractured basement lithological formations. Areas with moderate vulnerability to erosion occupy almost the entire surface area of the Amizmiz basin, covering 62% of the basin area. These areas are generally covered by moderately dense vegetation, which is not conducive to protecting the soil against the erosive effects of intense rainfall. The erodibility becomes low to very low in the eastern and northern parts of the basin, with area percentages of 13% and 6%, respectively. These areas are marked by the dominance of dense forests and low rainfall; they are also structurally less fractured than the axial zone, which contributes to reducing the erodibility in these areas.

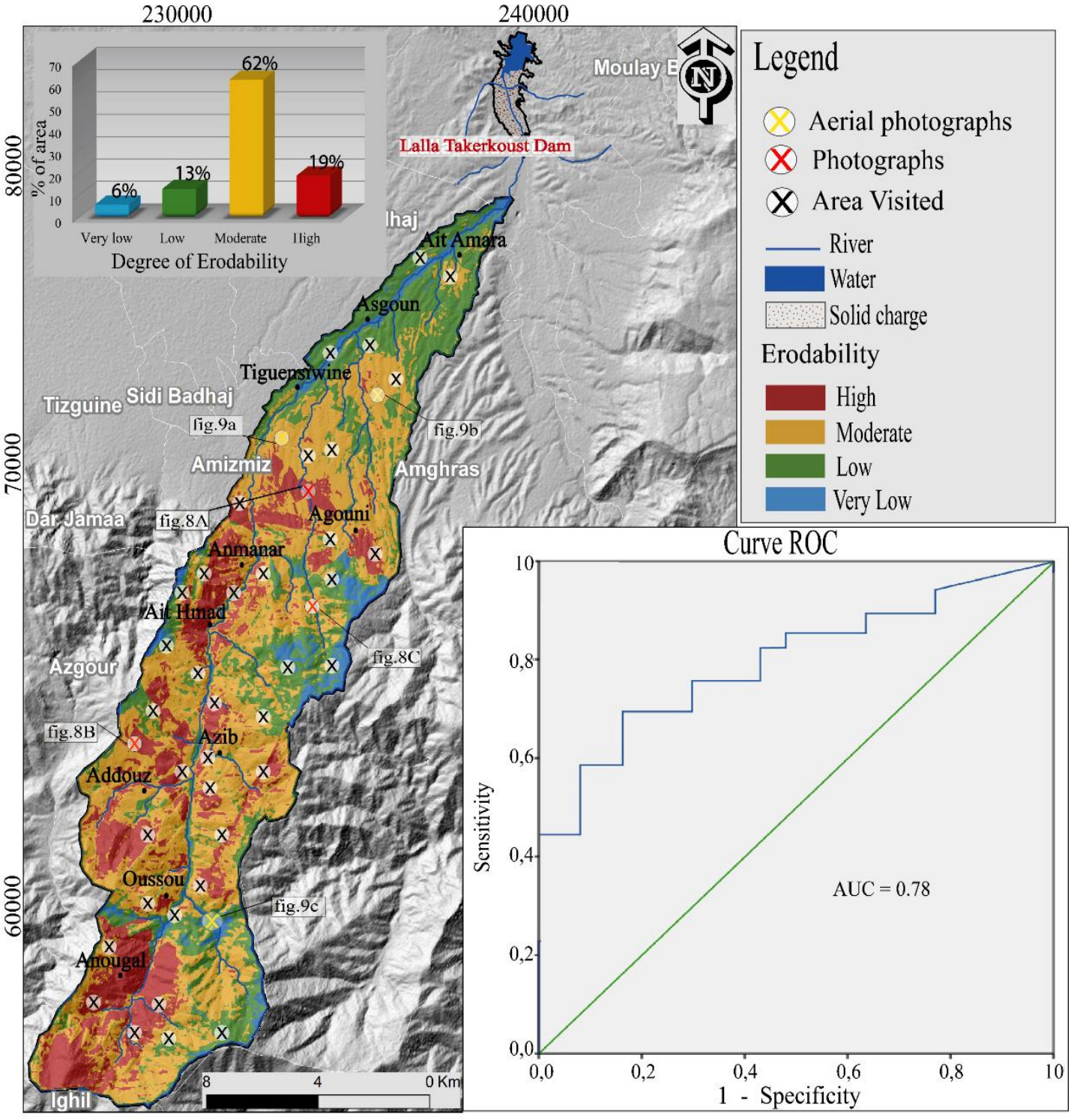

Figure 7. (A) Map of the erodibility of the Amizmiz watershed created using the MIF model; (B) ROC curve for validation of the MIF model.

3.3. Discussion

The results of this study indicate that the high susceptibility of soils to erosion in the axial and western zones of the Amizmiz watershed, which represent 19% of its area, is the result of a combination of factors influencing erodibility. The aggressive action of rainfall combined with the fragility of less-resistant soils represented by fractured shale and steep topography increases the soil vulnerability. The absence of vegetation cover in the axial zone also exacerbates the risk of erosion; however, the degree of erosion is considerable in the western zones despite the presence of dense vegetation cover. This is explained by the high weights attributed to the erosivity of precipitation and lithological factors compared with the weights of other factors, such as the vegetation density.

The decrease in soil vulnerability to erosion in the eastern part of the catchment, covering 9% of the total area, is mainly attributed to the erosivity of precipitation, which decreases from west to east in the catchment. The aggressiveness of precipitation is a major factor in triggering hydraulic erosion and can even attenuate the strong weighting of the lithological friability factor, particularly on low slopes. This is particularly true in the north of the Amizmiz Basin (13% of the total basin area), considering the low degree of erodibility despite the predominance of loose and friable alluvial and quaternary formations that are associated with low slopes and low precipitation erosivity, which reduces the occurrence of hydraulic erosion. These results confirm the strong interdependence between the factors used in the approach employed in this study.

The results of this study highlight the importance of managing the risks associated with water erosion in the Amizmiz Basin. This includes damage to infrastructure, such as siltation of the dam. The vulnerability of soils to erosion in the western and axial parts of the Amizmiz Basin does not exclude the downstream part from the problems associated with water erosion, such as the accumulation of solid load. Among the major damage caused by the risk of erosion in our study area is the silting of the Lalla Takerkoust Dam, located in the downstream part of the basin.

To evaluate the efficiency of the MIF model used in this study, we compared our results with those of the quantification and modelling of soil losses in the Western High Atlas areas located in proximity to our study area, which have the same lithological, topographical, and climatic characteristics as the Amizmiz Basin. Based on the results obtained by Kabili *et al.* (2023) in the Asif El mal catchment located to the west of the Amizmiz basin, soil losses are generally localised in the axial part of the catchment, which is marked by high precipitation, highly fractured basement formations, and degraded vegetation cover. To the east of the Amizmiz basin, Markhi *et al.* (2015) and Gourfi *et al.* (2024) studied the N'fis catchment and suggested that the greatest soil losses are recorded in the axial zone, with a rate of more than 301 t/ha/y (Gourfi *et al.,* 2023; 2019; Markhi *et al.,* 2015).

This significant soil destruction is essentially caused by a combination of factors that accelerate the erosion process, including the absence of vegetation. This phenomenon has been reported in several previous studies on soil erodibility on an international scale, e.g. in South Africa (Ebhuoma *et al.,* 2022), Tunisia (Khemiri *et al.,* 2021), and India (Saha *et al.,* 2022). According to a study by Khemiri (2021) that mapped soil erosion susceptibility in the N'oz Basin in South Africa, low vegetation cover in each area reduces the water retention capacity of the soil, which reduces the infiltration capacity and consequently increases runoff, thus increasing soil erodibility. In our study area, this manifests in ruined landscapes ravaged by runoff, particularly in clay formations. Another example is the study by Ebhuoma *et al.* (2022), who reported that high rainfall intensity combined with low vegetation cover causes the detachment of fine and coarse soil particles in the uThukela Basin in South Africa using the AHP model. Khemiri *et al.* (2021) used the MUSLE and RUSLE models in the Fidh Ali and Fidh Ben Naceur catchments in Tunisia and suggested that steep slopes associated with soft, friable formations with low permeability favour runoff and increase the risk of hydraulic erosion. This is particularly true in areas with high levels of agricultural and human activities (Khemiri *et al.,* 2021). In the same context, the results obtained by Saha *et al.* (2022) in central India based on machine learning algorithms demonstrated that soil erosion and vulnerability are more important on previously bare slopes and in the absence of vegetation cover in bare soils.

All of the results of these previous studies confirm the strong interdependence between the factors used in the method employed in this study. It is important to mention that the MIF model is a descriptive hydrogeological modelling approach that is used for the first time in our study to map the risk of water erosion. The results obtained and their validation confirm that this model is highly satisfactory and effective for identifying erosion-sensitive areas in the Amizmiz watershed. This

provides a better understanding of the dynamics and factors of erosion and can help ensure management of the risks and damage associated with the problem of erosion, such as silting of dams and deterioration in the quality of agricultural soil.

3.4. Validation

Validation of the model used for hydraulic erosion modelling in the Amizmiz watershed was a crucial step in our study. This validation helps establish a connection between the results generated by geospatial methods and the reality on the ground, considering geomorphological and climatic variations. Thus, this validation complements the contributions of remote sensing and GIS coupled with the MIF model for mapping areas vulnerable to erosion in the Amizmiz watershed. The validation method is based on field visits to sites specifically identified by GPS and featured on the erodibility map (Figure 7A); these sites were uniformly distributed throughout the basin from upstream to downstream. We obtained field photographs (Figure 8) and high-resolution aerial photographs (Figure 9) that illustrate the different classes of erodibility represented on the ground. Higher degrees of erodibility are manifested in bank degradation (Figure 8A), linear erosion in clay formations (Figure 8B), and the development of gully erosion in the downstream part of the watershed (Figure 9b). Mass erosion forms also occur in the concave part of the river due to the erosive effect, although the presence of moderately dense vegetation moderated the degree of erodibility (Figure 8C).

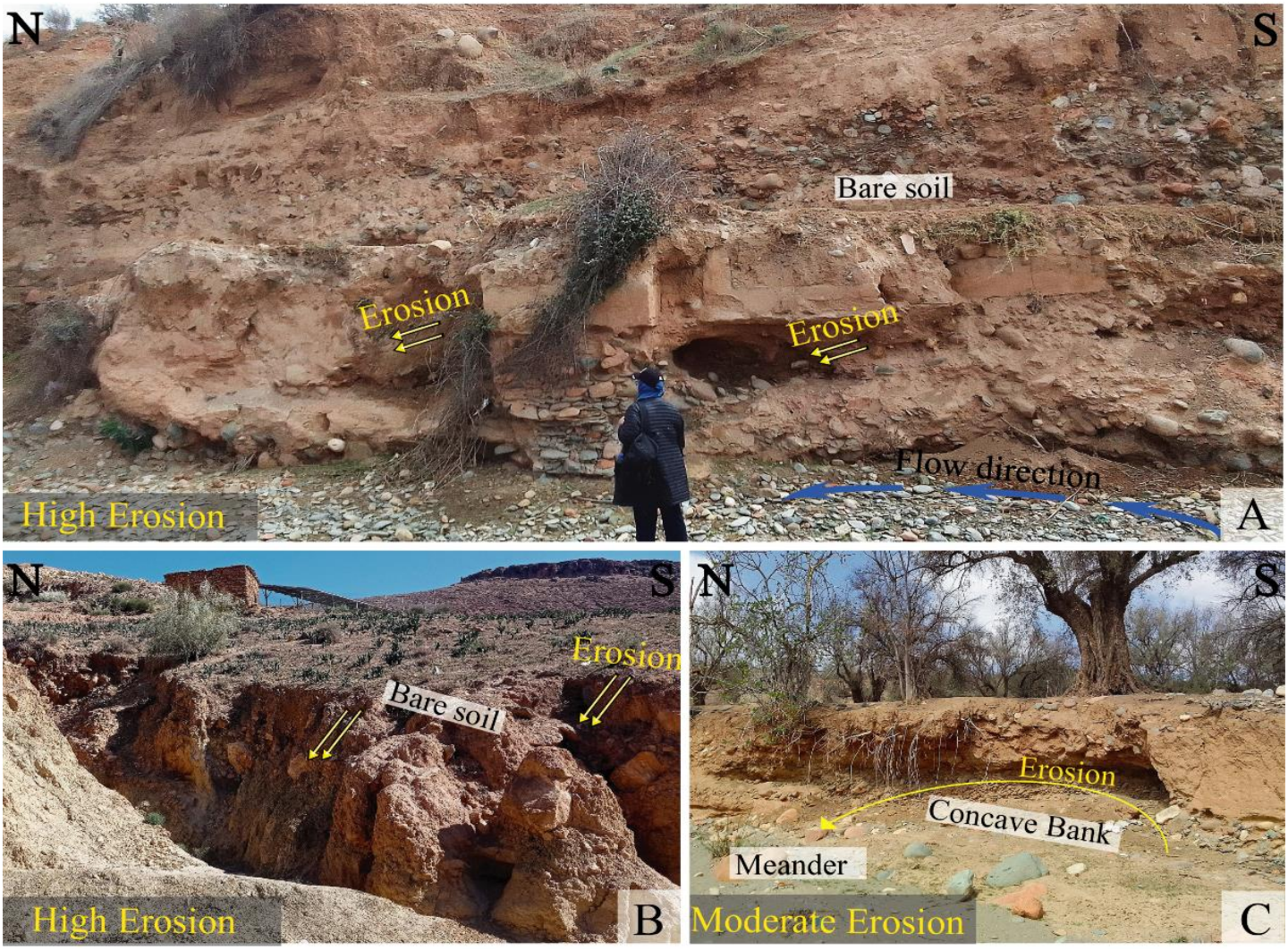

Figure 8. Field photographs of the Amizmiz watershed. (A) Bank degradation; (B) linear erosion in clay formations; (C) mass erosion of riverbanks.

Areas of low erodibility appear on the plains and in areas of abrupt change in slope, which favours accumulation rather than erosion, resulting in the development of alluvial cones (Figure 9a). Soil loss becomes increasingly low in areas of very dense plant cover, which can ensure that the soil remains stable, even near the river (Figure 9c). To assess the accuracy of the MIF method, we adopted Le Roux's classification, which is based on a comparison between the classes obtained in the field and those in the synthetic erodibility map (Le Roux *et al.,* 2008). By matching the

erodibility classes obtained from the MIF model with the corresponding erosion manifestations detected in the field, we found a strong concordance. To quantify this concordance, we used the ROC curve. This method allows for good evaluation of the performance of predictive models in binary classification situations, as is the case with this approach, in which it is necessary to distinguish eroded areas from non-eroded areas. This involves comparing the proportion of correct detections (sensitivity) to that of errors (1-specificity) based on various thresholds. The ROC curve is generated using SPSS statistical software (Figure 7B) utilising the observation data and predictive erodibility classes provided by the MIF model. The area under the curve (AUC), which measures the overall predictive capability of the model, is automatically obtained from the SPSS software and found to be 0.78. This indicates that in 78% of cases, the model correctly identifies an eroded area compared to a non-eroded area. According to several previous studies (Barakat *et al.,* 2023; Hitouri *et al.,* 2022; Lal *et al.,* 2001), this value indicates a very good predictive capability for hydraulic erosion modelling.

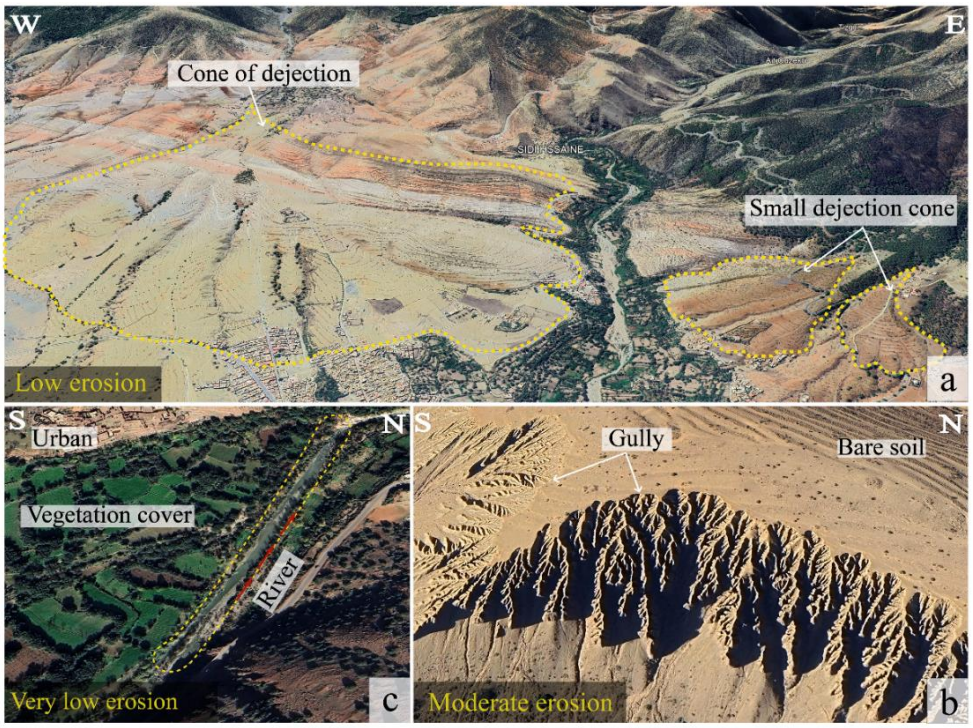

Figure 9. Aerial photographs of the Amizmiz watershed. (a) Development of alluvial cones on the plain; (b) development of gullies in clay formations; (c) very low erosion on the riverbanks.

4. Conclusion

Soil loss in the western High Atlas of Morocco is a serious environmental problem that affects sustainable development, reduces soil productivity, and promotes siltation of water reservoirs and dams. This study focuses on modelling the hydraulic erosion in the Amizmiz watershed located in the Western High Atlas, which is characterised by long periods of drought, intense and erosive precipitation, and particular topographic and lithological characteristics favouring soil degradation and loss. These conditions have led to the silting of the Lalla Takerkoust Dam located in the downstream part of the Amizmiz watershed, and consequently to a reduction in its storage capacity, highlighting the immediate necessity of modelling hydraulic erosion to attenuate these devastating effects. The multi-influencing factor (MIF) model adopted in this study in conjunction with remote sensing and GIS data allow us to identify the predominant factors influencing soil erodibility and identify the areas susceptible to hydraulic erosion in the Amizmiz watershed. The results highlight lithological factors, precipitation erosivity, and fracturing as the most significant factors triggering soil erosion. It is important to note that although the MIF model is dedicated to hydrogeological modelling, it has provided satisfactory results in modelling the risk of water erosion in the Amizmiz watershed. The results of this approach reveal that areas with a high susceptibility to erosion are mainly concentrated in the axial zone and western part of the lower basin, where the conditions are very favourable for soil erodibility, such as steep slopes and outcrops of basement shale that are strongly affected by fracturing and intense precipitation. In contrast, the downstream part of the basin is characterised by very gentle slopes and a low-toabsent degree of fracturing, which reduces the susceptibility to erosion despite the dominance of loose Quaternary

formations. These results underscore the urgency of implementing watershed management strategies to preserve natural resources and reduce the risks associated with erosion in the Western High Atlas region.

Acknowledgements

The researchers would like to thank the organisations that provided the data required for the study free of charge, including DIVA-GIS, OpenStreetMap, U.S. Geological Survey, NAZA website, and the Laboratory of Geoscience Geotourism Natural Hazards and Remote Sensing (2GRNT), the GEO-ANLY-SIS Morocco, engineering consulting office of Geological, geophysical, and environmental services, and the University of Cadi Ayyad for supporting this research.

Author Contributions

Conceptualisation: Saloua, A.; **methodology**: Saloua, A., Said, M., Abdelfattah, A., & Akram, E.; **investigation**: Saloua, A., Said, M., Abdelfattah, A., & Akram, E.; **writing—original draft preparation**: Saloua, A., Said, M., Abdelfattah, A., & Akram, E.; **writing—review and editing**: Ahmed, A., & Abdellah, A.; **visualisation**: Saloua, A. All authors have read and agreed to the published version of the manuscript.

Conflict of interest

The authors declare that they have no competing interests.

Data availability

Data is available upon request.

Funding

No specific funding must be declared for this work.

References

Agli, S., Ahmed, A., Abdellah, A., Abdelouahed, F., Moujane, S., Salma, K., & Maryam, E. (2024). Delineation of Groundwater Storage and Recharge Potential Zones Using Multi-Influencing Factors (MIF) Method: Application in Synclinal Coastal Basin of Essaouira (Western High Atlas of Morocco). *Geomatics and Environmental Engineering*, 18(4), 117–145. doi: 10.7494/geom.2024.18.4.117

Agli, S., Ahmed, A., Abdellah, A., Abdelouahed, F., Moujane,et al., (2023). Characterization the dynamics of transport of quartz grains in the Amizmiz watershed (Western High Atlas): Exoscopic approach. *International Journal of Advanced Natural Sciences and Engineering Researches (IJANSER*), 7(11), 552–560. doi: 10.59287/as-ijanser.716

Ayad, A., Ribeiro, M. L., Mata, J., Ferreira, P., Ezzouhairi, H., Charif, A., & Dias, R. (1998). Evolution du magmatisme cambrien en deux régions périgondwanniennes: Azegour (Haut-Atlas) et Alter do Chao-Elvas (NE Alentejo). *Communicaçaos do Instituto Geologico e Mineiro*, 84, B154-B157.

Barakat, A., Rafai, M., Mosaid, H., Islam, M. S., & Saeed, S. (2023). Mapping of water-induced soil erosion using machine learning models: a case study of Oum Er Rbia Basin (Morocco). *Earth Systems and Environment*, 7(1), 151-170. doi: 10.1007/s41748-023-003768

Chen, W., Shahabi, H., Zhang, S., Khosravi, K., Shirzadi, A., Chapi, K., ... & Ahmad, B. B. (2018). Landslide susceptibility modelling based on gis and novel bagging-based kernel logistic regression. *Applied Sciences*, 8(12), 2540. doi: 10.3390/app8122540

Ebhuoma, E. E. (2022). Factors undermining the use of seasonal climate forecasts among farmers in south africa and zimbabwe: Implications for the 1st and 2nd sustainable development goals. *Frontiers in Sustainable Food Systems*, 6, 761195. doi: 10.3389/fsufs.2022.761195

Ebhuoma, O., Gebreslasie, M., Ngetar, N. S., Phinzi, K., & Bhattacharjee, S. (2022). Soil erosion vulnerability mapping in selected rural communities of uThukela catchment, South Africa, using the analytic hierarchy process. *Earth Systems and Environment*, 6(4), 851-864. doi: 10.1007/s41748-022-00339-0

Elbadaoui, K., Mansour, S., Ikirri, M., Abdelrahman, K., Abu-Alam, T., & Abioui, M. (2023). Integrating Erosion Potential Model (EPM) and PAP/RAC Guidelines for Water Erosion Mapping and Detection of Vulnerable Areas in the Toudgha River Watershed of the Central High Atlas, Morocco. *Land*, 12(4), 837. doi: 10.3390/land12040837

Ellero, A., Ottria, G., Malusà, M. G., & Ouanaimi, H. (2012). Structural geological analysis of the High Atlas (Morocco): evidence of a transgressional fold-thrust belt. *Tectonics-recent advances*, 229-258.

Errami, M., Algouti, A., Algouti, A., Farah, A., & Agli, S. (2023). Utilization of ASTER data in lithological and lineament mapping of the southern flank of the Central High Atlas in Morocco. *Geologos*, 29(1), 1-20. doi: 10.2478/logos-2023-0001

Farah, A., Algouti, A., Algouti, A. (2021). Lineament mapping in the Iknioun area (eastern anti-atlas, Morocco) using Landsat-8 Oli and SRTM data. *Remote sensing applications: society and environment*, 23, 100606. doi: 10.1016/j.rsase.2021.100606

Farah , A., Algouti, A., Algouti, A., et al., (2022). GIS and remote sensing coupled with analytical hierarchy process (AHP) for the selection of appropriate sites for landfills: a case study in the province of Ouarzazate, Morocco. *Journal of Engineering and Applied Science,* 69(1), 19. doi: 10.1186/s44147-022-00019-8

Farah, A., Algouti, A., Algouti, A., Ait Mlouk, M., & Ifkirne, M. (2022). Lineament mapping in the Central High Atlas using ASTER and ASTER-GDEM data,(Morocco). *Boletín de la Sociedad Geológica Mexicana*, 74(1). doi: 10.18268/BSGM2022v74n1a2

Fartas, N., El Fellah, B., Mastere, M., Benzougagh, B., & El Brahimi, M. (2022). Potential soil erosion modeled with RUSLE approach and geospatial techniques (GIS tools and remote sensing) in Oued Joumouaa watershed (Western Prerif-Morocco). *The Iraqi Geological Journal*, 47-61.

Forootan, E. (2022). Erosion susceptibility assessment using fuzzy logic and multi-influencing factors combination approach. *Arabian Journal of Geosciences*, 15(5), 444. https://doi.org/10.1007/s12517-022-09875-2

Gourfi, A., & Daoudi, L. (2019). Effects of land use changes on soil erosion and sedimentation of dams in semi-arid regions: example of N'fis watershed in western high atlas, Morocco. *J Earth Sci Clim Change*, 10(513), 2. doi: 10.4172/2157-7617.1000513

Gourfi, A., Daoudi, L., Daoud, N. B., & Fagel, N. (2024). Clay minerals in soils and sediment as tracers of provenance: The case study of the N'fis watershed, Morocco. *Soil Use and Management*, 40(1), e12925.

Haitami, H., Ulfa, A., & Muntaha, A. (2017). Kadar vitamin C jeruk sunkist peras dan infused water. *Medical Laboratory Technology Journal*, 3(1), 22-26. doi: .33086/mltj.v3i1.71

Hitouri, S., Varasano, A., Mohajane, M., Ijlil, S., Essahlaoui, N., Ali, S. A., ... & Teodoro, A. C. (2022). Hybrid machine learning approach for gully erosion mapping susceptibility at a watershed scale. ISPRS *International Journal of Geo-Information*, 11(7), 401. doi: 10.3390/ijgi11070401

Igwe, O., John, U. I., Solomon, O., & Obinna, O. (2020). GIS-based gully erosion susceptibility modelling , adapting bivariate statistical method and AHP approach in Gombe town and environs Northeast Nigeria. *Geoenvironmental Disasters*, 7, 1-16.

Innan, R., & Moustaghfir, K. (2012). Predicting Employees' Behavior: An Application of the Theory of Planned Behavior; The Case of the Moroccan Forestry Department (HCEFLCD). *In Proceedings of the Management, Knowledge and Learning International Conference*, 333-348.

Kabili, S., Ahmed, A., Abdellah, A., & Akram, E. G. (2023). Quantification of water erosion using empirical models RUSLE and EPM in the Rheraya basin in the High Atlas of Marrakech. *Disaster Advances*, 16(5), 19-28.

Kabili, S., Ahmed, A., Abdellah, A., & Salma, E. (2023). Estimation and mapping of water erosion and soil loss: Application of Gavrilovic erosion potential model (EPM) using GIS and remote sensing in The Assif el mal Watershed, Western high Atlas. *China Geology*, 7, 1-14. doi: 10.31035/cg2023058

Ke, Y., Im, J., Lee, J., Gong, H., & Ryu, Y. (2015). Characteristics of Landsat 8 OLI-derived NDVI by comparison with multiple satellite sensors and in-situ observations. *Remote sensing of environment,* 164, 298-313. doi: 10.1007/s12665-023-10768-5

Khairuddin, W. N. B. W., Rambat, S. B., & Harun, A. N. B. (2022). Community based index of coastal erosion using ahp analysis. *IOP* Conference Series: *Earth and Environmental Science*, 1091(1), 012042.

Khemiri, K., & Jebari, S. (2021). Évaluation de l'érosion hydrique dans des bassins versants de la zone semi-aride tunisienne avec les modèles RUSLE et MUSLE couplés à un Système d'information géographique. *Cahiers Agricultures*, 30, 7.

Kirkby, M. (2003). Modelling erosion–the PESERA project. In The First SCAPE Workshop: *Alicante*, Spain.

Kirkby, M., Jones, R. J., Irvine, B., Gobin, A. G. G., Cerdan, O., van Rompaey, J. J., ... & Huting, J. R. M. (2004). Pan-European Soil Erosion Risk Assessment for Europe: the PESERA map, version 1 October 2003. Explanation of Special Publication Ispra 2004 No. 73 (SPI 04.73) (No. 16, 21176). *Office for Official Publications of the European Communities*.

Lal, R. A. T. T. A. N. "Soil degradation by erosion." *Land degradation & development* 12.6 (2001): 519-539. doi: 10.1002/ldr.472

Le Bissonnais, Y., Thorette, J., Bardet, C., & Daroussin, J. (2002). L'érosion hydrique des sols en France. *Rapport INRA, IFEN*, 106.

Le Roux, J. J., Morgenthal, T. L., Malherbe, J., Pretorius, D. J., & Sumner, P. D. (2008). Water erosion prediction at a national scale for South Africa. *Water* Sa, 34(3), 305-314. doi : 10.4314/wsa.v34i3.183650

Lin, L., & Pussella, P. (2017). Assessment of vulnerability for coastal erosion with GIS and AHP techniques case study: Southern coastline of Sri Lanka. *Natural Resource Modelling* , 30(4), e12146.

Liu, J., Gao, G., Wang, S., Jiao, L., Wu, X., & Fu, B. (2018). The effects of vegetation on runoff and soil loss: Multidimensional structure analysis and scale characteristics. *Journal of Geographical Sciences*, 28, 59-78.

Lu, D., Li, G., Valladares, G. S., & Batistella, M. (2004). Mapping soil erosion risk in Rondonia, Brazilian Amazonia: using RUSLE, remote sensing and GIS. *Land degradation & development*, 15(5), 499-512. doi: 10.1002/ldr.634

Mandal, K., Saha, S., & Mandal, S. (2021). Applying deep learning and benchmark machine learning algorithms for landslide susceptibility modelling in Rorachu river basin of Sikkim Himalaya, India. *Geoscience Frontiers*, 12(5), 101203. doi: 10.1016/j.gsf.2020.101203

Mandal, P., Saha, J., Bhattacharya, S., & Paul, S. (2021). Delineation of groundwater potential zones using the integration of geospatial and MIF techniques: A case study on Rarh region of West Bengal, India. *Environmental Challenges*, 5, 100396. doi: 10.1016/j.envc.2021.100396

Markhi, A., Laftouhi, N., Grusson, Y., & Soulaimani, A. (2019). Assessment of potential soil erosion and sediment yield in the semi-arid N′ fis basin (High Atlas, Morocco) using the SWAT model. *Acta Geophysica*, 67, 263-272. doi: 10.1007/s11600-018-0200-6

Merkhi, A., Laftouhi, N. E., Soulaimani, A., & Fniguire, F. (2015). Quantification et évaluation de l'érosion hydrique en utilisant le modèle RUSLE et déposition intégrée dans un SIG. Application dans le bassin versant n'fis dans le haut atlas de Marrakech (Maroc). *Eur Sci J* 11 (29): 340–356.

Moujane, S., Algouti, A., Algouti, A., Farah, A., Aboulfaraj, A., & Nafouri, I. (2024). Mapping lineaments using Landsat 8 OLI and SRTM data; a case study of the eastern part of the Ouarzazate Basin, Morocco. *Journal of Mountain Science*, 21(3), 987-1003. doi: 10.1007/s11629-024-7426-7

Najia, F., Bouchta, E., Mohamed, M., Benzougagh, B., & El Brahimi, M. (2021). Evaluation of water erosion by mapping and application of the PAP/RAC method in the Prerif of Ouazzane. *Ecology, Environnement and Conservation*, 12.

Nouaim, W., Rambourg, D., El Harti, A., Abderrahim, E., Merzouki, M., & Karaoui, I. (2023). The estimation of water erosion with RUSLE and deposition model: A case study of the Bin El-Ouidane dam catchment area (High Atlas, Morocco). *Journal of Water and Land Development*. doi: 10.24425/jwld.2023.141424

Oudchaira, S., Rhoujjati, A., Hanich, L., & EL Hachimi, M. L. (2024). Evaluating soil loss and sediment yield for sustainable management of the Hassan II dam within Morocco's Upper Moulouya watershed using RUSLE model and GIS. *Environmental Earth Sciences,* 83(7), 210. doi: 10.1007/s12665-023-10768-5

Ourhzif, Z., & Algouti, A., Algouti, A., Ait Mlouk, M., Aydda, A., (2020). Soil Erosion susceptibility mapping using support vector machine and Remote sensing data in Semi-arid Environment: South High Atlas of Marrakech (Morocco). *Ecology Environment and Conservation*, 27(2), 405-421.

Rajasekhar, M., Raju, G. S., Sreenivasulu, Y., & Raju, R. S. (2019). Delineation of groundwater potential zones in semi-arid region of Jilledubanderu river basin, Anantapur District, Andhra Pradesh, India using fuzzy logic, AHP and integrated fuzzy-AHP approaches. *HydroResearch*, 2, 97-108. doi: 10.1016/j.hydres.2019.10.001

Saha, S. M., Pranty, S. A., Rana, M. J., Islam, M. J., & Hossain, M. E. (2022). Teaching during a pandemic: do university teachers prefer online teaching?. *Heliyon*, 8(1). doi: 10.1016/j.heliyon.2021.e08834

Saha, S., Sarkar, D., & Mondal, P. (2022). Assessing and mapping soil erosion risk zone in Ratlam District, central India. *Regional Sustainability*, 3(4), 373-390.

Saoud, M., & Meddi, M. (2022). Mapping of erosion using USLE, GIS and remote sensing in Wadi El Hachem Watershed (Northern Algeria): Case study. *Journal of the Indian Society of Remote Sensing*, 50(3), 569-581.

Sutradhar, S., Mondal, P., & Das, N. (2021). Delineation of groundwater potential zones using MIF and AHP models: a micro-level study on Suri Sadar Sub-Division, Birbhum District, West Bengal, India. *Groundwater for Sustainable Development,* 12, 100547. doi: 10.1016/j.gsd.2020.100547

Tahouri, J., Sadiki, A., Karrat, L. H., Johnson, V. C., weng Chan, N., Fei, Z., & Te Kung, H. (2022). Using a modified PAP/RAC model and GIS-for mapping water erosion and causal risk factors: Case study of the Asfalou watershed, Morocco. *International Soil and Water Conservation Research,* 10(2), 254-272.

Valentin, C. (1994). Sécheresse et érosion au Sahel. *Sécheresse,* 5(3), 191-198.

Vanguestaine, M., & Van Looy, J. (1983). Acritarches du Cambrien moyen de la vallée de Tacheddirt (Haut-Atlas, Maroc) dans le cadre d'une nouvelle zonation du Cambrien. *Annales de la Société géologique de Belgique*.

Wischmeier, W. H., & Smith, D. D. (1965). Predicting rainfall-erosion losses from cropland east of the Rocky Mountains: Guide for selection of practices for soil and water conservation. *Agricultural Research Service, US Department of Agriculture,* 282.

Xu, D., & Guo, X. (2014). Compare NDVI extracted from Landsat 8 imagery with that from Landsat 7 imagery. *American Journal of Remote Sensing*, 2(2), 10-14. doi: 10.11648/j.ajrs.20140202.11

Yariyan, P., Janizadeh, S., Van Phong, T., Nguyen, H. D., Costache, R., Van Le, H., ... & Tiefenbacher, J. P. (2020). Improvement of best first decision trees using bagging and dagging ensembles for flood probability mapping. *Water Resources Management*, 34, 3037-3053. doi: 10.1007/s11269-020-02564-2

Ziadi, K., Barakat, A., El Aloui, A., Ouayah, M., & Namous, M. (2023). Modelling and mapping of soil erosion risk based on GIS and PAP/RAC guidelines in the watershed of Tassaoute (Central High-Atlas, Morocco). *Bulletin of Geography. Physical Geography Series*, (24), 65-83.